Pergamon

Int. J. Heat Mass Transfer. Vol. 39, No. 13, pp. 2846–2852, 1996

0017-9310/96 $15.00+0.00

0017-9310(95)00349-5

Flow and transport in a multilayered fluid system—II. Influence of thermal boundary conditions and encapsulant

J.-P. FONTAINE† and R. L. SANI

Center for Low-Gravity, Department of Chemical Engineering, University of Colorado, Boulder, CO 80309, U.S.A.

(*Received* 22 *February* 1993 *and in final form* 28 *July* 1995)

INTRODUCTION

The first part of this study modeled the flow and concomitant thermal transport in a differentially heated cavity containing two immiscible, shallow layers of high Prandtl number liquids. The numerical model was utilized to support a space experiment [see Part I], which was designed to investigate the thermocapillary convection generated at the interface between two fluids. One aim of the space experiment is to find criteria to reduce the surface tension driven flow in the lower liquid layer which is presumed to be representative of an encapsulated melt of an electronic material, although presently no low Prandtl number fluids are being investigated experimentally. This work was performed in collaboration with the ground-based experiments in progress by Koster [1, 2]. It is shown in Part I that the strength of the flow in the lower layer can be reduced by the use of encapsulation, both under terrestrial and micro-g conditions. The influence of the thermal boundary conditions and of another encapsulant liquid which is an order of magnitude more viscous than water is examined in this paper.

PHYSICAL MODEL

The configuration consists of two immiscible liquid layers of equal volume contained in a two-dimensional open cavity. An aspect ratio of $A = H/L = 1/5.1$ (where H is the height and L the length) representing Koster's experiments [1, 2] has been considered for each layer. A temperature gradient is imposed perpendicular to the gravitational force (1-g environment) by maintaining the isothermal side walls at different temperatures. The upper interface is taken to be a free surface, representative of a liquid–gas interface. Both the top and the intermediate liquid–liquid interface are deformable with fixed contact angles ($\phi = \pi/2$), and subjected to surface tension gradients induced by the temperature gradient along each interface. Both the free surface and the bottom are adiabatic. The fluids considered were the fluorinert FC75 for the lower layer and water or ethylene glycol for the upper one.

The mathematical and numerical models are described in Part I. The simulations were performed with the FIDAP code [3] based on a Galerkin finite element (GFE) technique.

EFFECT OF THE THERMAL BOUNDARY CONDITIONS

The investigation of different thermal boundary conditions was performed for comparisons with the experimental results of Koster [1, 2], viz at the free surface, the bottom of the cavity, and at the singular nodes located at the intersection between the vertical walls and the free surface. The combination fluorinert FC75–water (used in Part I) is considered. These effects were studied numerically employing a 73×59 mesh [see Part I] for overall temperature gradient ($\Delta T = 1.1$K): $Gr_1 = 3 \times 10^6$, $Ma_1 = 5.1 \times 10^4$, $Pr_1 = 23.38$, $Ca_{01} = 6.46 \times 10^{-5}$, $Gr_2 = 2.7 \times 10^5$, $Ma_2 = 8.3 \times 10^4$, $Pr_2 = 7.32$, $Ca_{02} = 3.65 \times 10^{-5}$ and $Fr = 1.4 \times 10^{-5}$. We recall from Part I that with an adiabatic free surface the system exhibits a two large co-rotating cell structure with a thin shear layer inbetween, located at the bottom of the upper layer. The thermocapillary forces on the free surface cause the appearance of three internal co-rotating cells in the upper layer. (See Part I for more details.)

Non-adiabatic free surface

A configuration considering heat loss by convection at the free surface was investigated. This convective heat transfer is modeled by varying the Nusselt number in a Newtonian heat transfer model. In this case the dimensionless adiabatic condition [equation (19)] given in the mathematical model [see Part I] is replaced by:

$$-\hat{\mu}\frac{1}{Pr_2 R_{\sigma_2}^{2/3}}\mathbf{n}_2 \cdot \nabla T_2 = \hat{\mu}\frac{1}{Pr_2 R_{\sigma_1}^{2/3}} Nu_2 T_2 \qquad (19\text{bis})$$

where

$$\hat{\mu} = \frac{\mu_2}{\mu_1}, \quad Nu_j = \frac{h_{cj}L}{k_j}$$

is the Nusselt number, k is the thermal conductivity and h_c is the convective heat transfer coefficient.

Major changes in the flow structure of the upper layer were obtained. When gradually increasing the Nusselt number from 0 (corresponds to an adiabatic condition) up to 5, one can first observe the disappearance of the third internal cell in the top layer. Then the second cell moves toward the cold wall, followed by a decrease in size and intensity of this cell before a unicellular flow fills the upper layer, still being accelerated at the free surface near the hot wall. This behavior of the flow might be another reason why the three internal co-rotating cell structure obtained in Section 5.1 of Part I with an adiabatic free surface is not seen experimentally [1, 2]; an insulated free surface seems to be a too idealized model. Figure 1(a, b) displays the streamline and isotherm patterns for $Nu_2 = 2.3$: the second internal cell (near the cold wall) is weak, and the main cell extends over half the cavity. The thickness of the separation zone (shear layer between the two co-rotating cells of the upper and lower layers) underneath this main cell decreases. Along the free surface a slight reduction in the temperature gradient occurs at the cold wall.

Increasing the Nusselt number, the second internal co-

† Institut de Mécanique des Fluides, C.N.R.S.-U.M.34 and I.R.P.H.E., C.N.R.S.-U.M.138, 1, rue Honnorat, 13003 Marseille, France.

NOMENCLATURE

$A = H/L$ aspect ratio of each liquid layer
Ca Capillary number
Fr Froude number
Gr Grashof number
H height of each liquid layer
L length of the cavity
Ma Marangoni number
Pr Prandtl number
R_σ surface tension Reynolds number
Nu Nusselt number
T temperature
g gravitational acceleration
k thermal conductivity
h_c convective heat transfer coefficient
u horizontal component of the velocity
v vertical component of the velocity
$\mathbf{n}$ unit outward pointing normal vector.

Greek symbols
ϕ contact angle of a liquid
μ dynamic viscosity
ρ density
χ thermal diffusivity
σ surface tension coefficient.

Subscript
0 reference state
1 lower layer ($j = 1$ or 2)
2 upper layer.

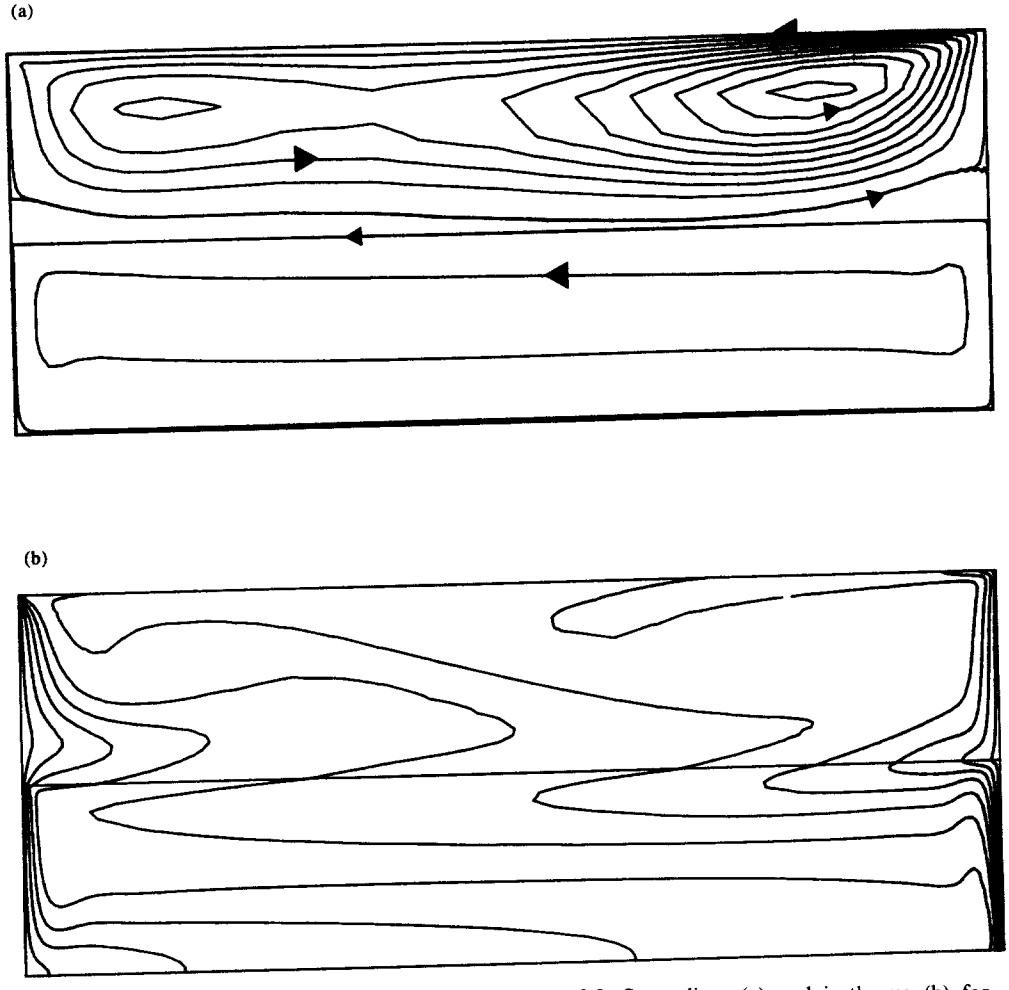

Fig. 1. Convective heat loss at the free surface: $Nu_2 = 2.3$. Streamlines (a) and isotherms (b) for $Gr_1 = 3 \times 10^6$, $Ma_1 = 5.1 \times 10^4$, $Pr_1 = 23.38$, $Ca_{01} = 6.46 \times 10^{-5}$, $Gr_2 = 2.7 \times 10^5$, $Ma_2 = 8.3 \times 10^4$, $Pr_2 = 7.32$, $Ca_{02} = 3.65 \times 10^{-5}$, and $Fr = 1.4 \times 10^{-5}$. $\Psi_{Max} = 4.64 \times 10^{-2}$; $\Psi_{min} = -2.42 \times 10^{-3}$.

rotating cell disappears in the upper layer. When $Nu_2 = 5$, a relatively large value, the unicellular flow described above is seen in the upper layer [Fig. 2(a–d)]. The center of the main cell is located near the hot wall and reflects the acceleration imparted to the fluid by the thermocapillary forces at the free surface. This motion induces an extremely thin separation zone between about $L/2$ and $3L/4$. This compression of the layer results from very small velocities along the liquid–liquid interface, the local minimum is nearly zero [Fig. 2(c)]. In the case of an insulated free surface, we obtained a relatively uniform velocity profile along the liquid–liquid interface for more than half of the length in the central region and larger velocities; the maximum velocity peak at the liquid–liquid interface close to the cold wall was 14% larger (see Table 1). This is caused by the decrease in the thermal gradient near this cold wall from $\Delta T/3$ to $\Delta T/4$ when considering heat loss (ΔT is the overall thermal gradient applied to the cavity). At the free surface the thermal gradient near the cold wall decreases from $2\Delta T/3$ (adiabatic) to more than $\Delta T/3$ with heat loss. This causes a reduction in the maximum velocity at the free surface (also maximum of the whole cavity) by 22% (see Table 1). Figure 2(d) shows a strong velocity close the hot wall: this second peak is increased by 41% compared to the adiabatic free surface case, leading to a much sharper thermal gradient near the hot wall. At the liquid–liquid interface the velocity close to the hot wall is only increased by 10%, due to only a slightly larger temperature gradient. The isotherms [Fig. 2(b)] appear 'S' shaped in the central region of the cavity in the upper layer. That is not the case with an insulated free surface where the upper portion of the isotherms is pulled toward the cold wall.

The effect of the thermal boundary condition imposed at the bottom of the cavity was analyzed for the previous configuration (heat loss at the free surface: $Nu_2 = 5$) by replacing the adiabatic condition by a 'theoretical' linear temperature profile at the bottom. The flow is not significantly affected. The magnitude of the temperature gradient is slightly increased near the cold wall, particularly at the liquid–liquid interface (about 5%), and slightly decreased near the hot wall. This results in an increase of the maximum velocity near the cold wall by 3% at the free surface and 2% at the liquid–liquid interface, and a decrease of the maximum velocities near the hot wall by 2% at the liquid–liquid interface and 5% at the free surface.

Free temperature at the upper corner nodes

As suggested by Chait [4], a weaker thermal condition was investigated at the upper corner nodes, viz. namely, where the isothermal walls and the free surface intersect. At these singular nodes the temperature was not imposed at the corresponding vertical wall temperature as done previously, but calculated by the numerical model via the assumed heat transfer mechanism.

Looking at the streamline and isotherm patterns, no noticeable change is seen: the transport is similar. However an important effect is the temperature obtained at these singular nodes. While the 'hot node' (top of the hot wall) is decreased by less than $2\Delta T/1000$, the 'cold node' (top of the cold wall) is increased by 22% of ΔT (ΔT is the total temperature gradient). This last result means that 22% of the overall temperature gradient between the heated walls occurs between the two first vertical nodes at this cold wall. We recall that the mesh is highly refined in this region, so that these two nodes are separated by about $\Delta y = 5.3L/10^4$. Thus, the peak of the maximum velocity (close to the cold wall) is decreased by 11%, while the secondary peak present near the hot wall is of same magnitude. This reduction of the velocity field near the cold wall disappears inside the upper layer, indeed at the liquid–liquid interface the maximum velocity is decreased by about 1%.

In conclusion, the model where the temperature at these singular nodes is fixed appears to be somewhat more realistic because in the alternative case 22% of overall ΔT occurs over such a small distance ($5.3L/10^4$) and since a strong corner boundary layer structure will exist in the cold wall-free surface corner. In any case this was the boundary condition of choice herein.

FLUORINERT FC75–ETHYLENE GLYCOL MODEL AT 1 *g*

In order to determine a better encapsulant liquid, a fluorinert FC75–ethylene glycol system was also studied at 1 *g* with ethylene glycol, $Pr_2 = 200.9$, as the upper layer. The main difference compared to water is its viscosity: $\mu_{eth} \approx 21\ \mu_{wat}$ (where the subscripts eth and wat denote ethylene glycol and water). The other fluid properties are comparable: $\rho_{eth} \approx 1.1\ \rho_{wat}$, $\chi_{eth} \approx 0.7\chi_{wat}$,

$$\frac{\partial \sigma_{eth}}{\partial T} \approx 1.9 \frac{\partial \sigma_{wat}}{\partial T}.$$

The flow structure in this configuration was examined for a sequence of imposed lateral thermal gradient up to $\Delta T = 10$ K. The 73×59 mesh was used.

Figure 3(a–d) displays the flow patterns obtained for a thermal gradient $\Delta T = 1.1$ K, viz. the largest considered for the fluorinert FC75–water system: $Gr_1 = 3 \times 10^6$, $Ma_1 = 3.7 \times 10^4$, $Gr_2 = 2.4 \times 10^3$, $Ma_2 = 2.5 \times 10^3$. The streamlines exhibit mainly a two co-rotating cell structure, one in each layer. The major change compared to the fluorinert-water system is that a stronger motion exists in the lower layer than in the upper one; this occurs due to the highly viscous nature of ethylene glycol. In the lower layer the streamlines and isotherms also exhibit a horizontally stratified structure [Fig. 3(a, b)]. In the upper layer an elongated cell with its center located near the cold wall is observed. The isotherms reflect a stronger convective flow near the cold wall than near the hot one. The maximum velocity in the entire cavity occurs in the descending stream along the cold wall in the lower layer; it is located at the free surface near the cold wall for the fluorinert–water system, showing a stronger influence of the surface tension gradient. The thermocapillary forces generated at the free surface cause a strong temperature gradient near the cold wall where half of the overall temperature gradient occurs. We recall that more than 60% of the global gradient occurs there in the water encapsulant layer and the slope of the gradient is steeper. Near the hot wall a weak thermal gradient appears.

Table 1. Maximum of the velocity field in the lower layer (fluorinert FC75) $U_{1,max}$ and in the upper layer $U_{2,max}$

		$\Delta T = 0.36$ K		$\Delta T = 1.1$ K	
		$U_{1,max}$ [cm s^{-1}]	$U_{2,max}$ [cm s^{-1}]	$U_{1,max}$ [cm s^{-1}]	$U_{2,max}$ [cm s^{-1}]
Single layer FC75	1-g_0	0.2395		0.6527	—
FC75–water	1-g_0	0.0413	0.5476	0.1041	1.5138
FC75–ethylene glycol	1-g_0	0.0374	0.0131	0.0713	0.0373
FC75–water | $Nu = 5$	1-g_0			0.09	1.1769

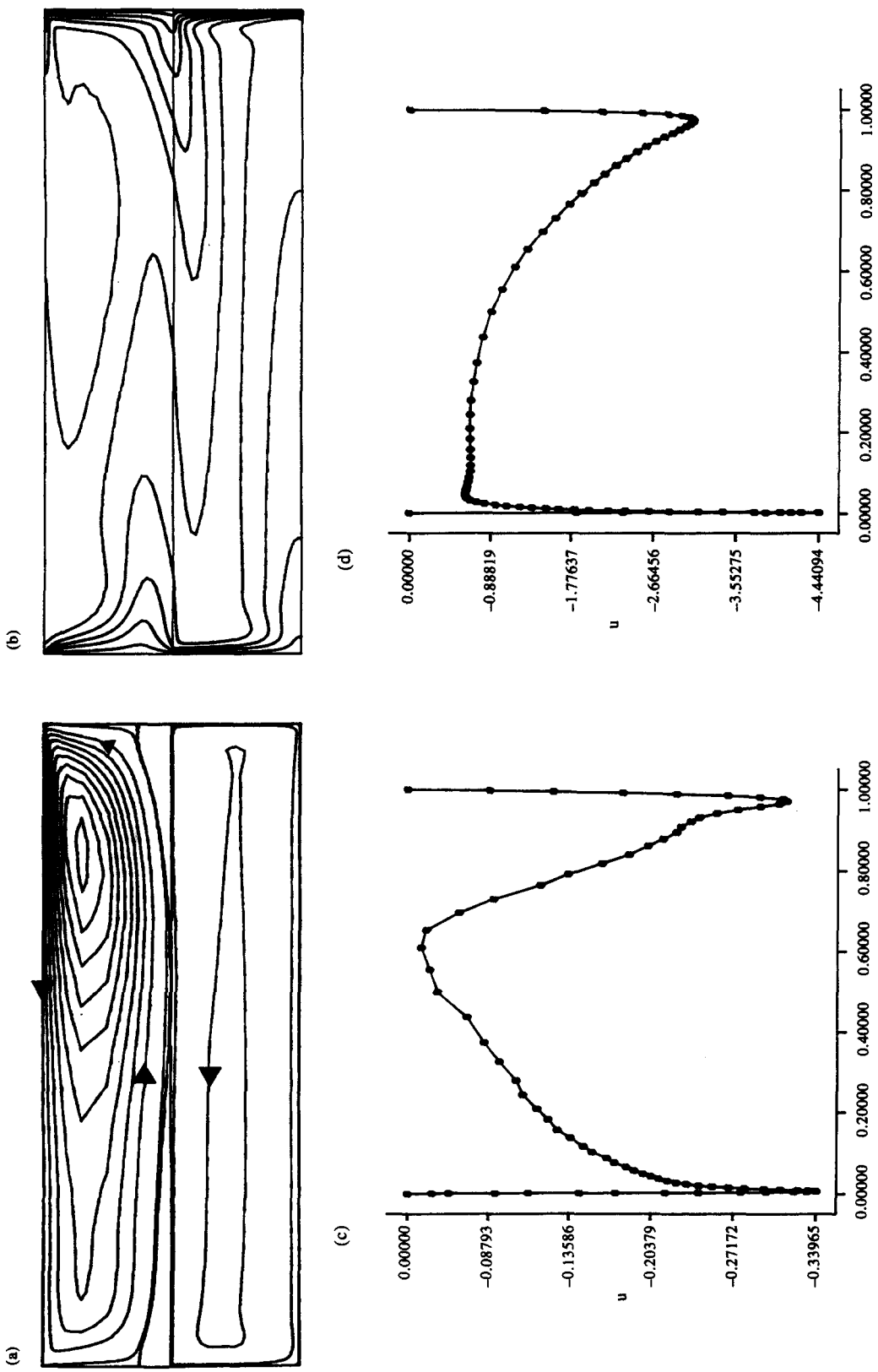

Fig. 2. Convective heat loss at the free surface: $Nu_2 = 5$. Streamlines (a), isotherms (b), and horizontal velocity profiles along the liquid–liquid interface (c) and the free surface (d) for $Gr_1 = 3 \times 10^6$, $Ma_1 = 5.1 \times 10^4$, $Pr_1 = 23.38$, $Ca_{01} = 6.46 \times 10^{-5}$, $Gr_2 = 2.7 \times 10^5$, $Ma_2 = 8.3 \times 10^4$, $Pr_2 = 7.32$, $Ca_{02} = 3.65 \times 10^{-5}$ and $Fr = 1.4 \times 10^{-5}$. $\Psi_{Max} = 5.45 \times 10^{-2}$, $\Psi_{min} = -2.56 \times 10^{-3}$.

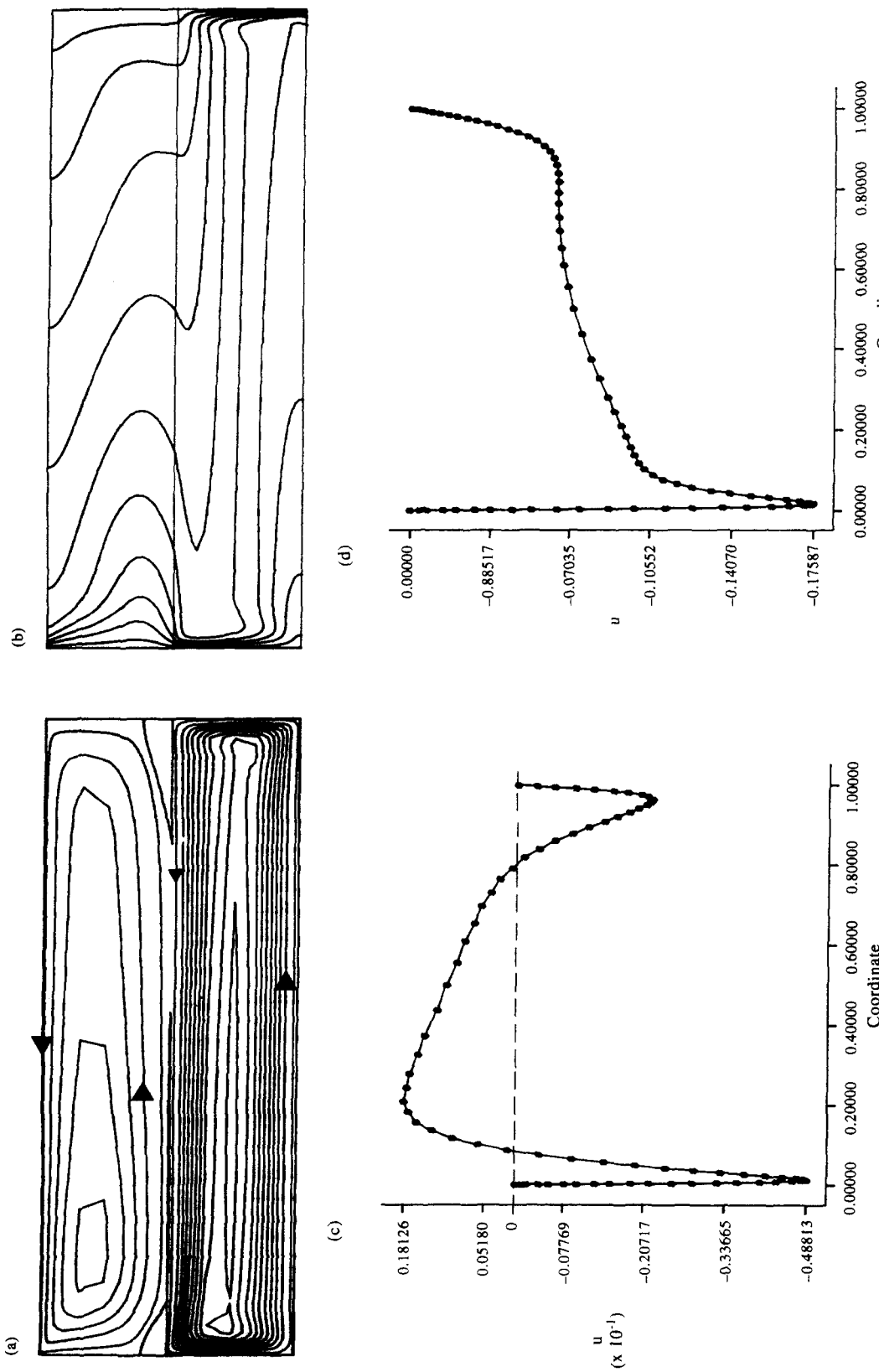

Fig. 3. Fluorinert FC75-ethylene glycol system for $\Delta T \approx 1.1$ K at 1 g: $Gr_1 = 3 \times 10^6$, $Ma_1 = 3.7 \times 10^4$, $Pr_1 = 23.38$, $Ca_{01} = 5.17 \times 10^{-3}$, $Gr_2 = 2.4 \times 10^5$, $Ma_2 = 2.5 \times 10^3$, $Pr_2 = 200.9$, $Ca_{02} = 5.33 \times 10^{-2}$ and $Fr = 9 \times 10^{-6}$. Streamlines (a), isotherms (b), and horizontal velocity profiles along the liquid–liquid interface (c) and the free surface (d). $\Psi_{Max} = 7.79 \times 10^{-3}$; $\Psi_{min} = -2.02 \times 10^{-4}$.

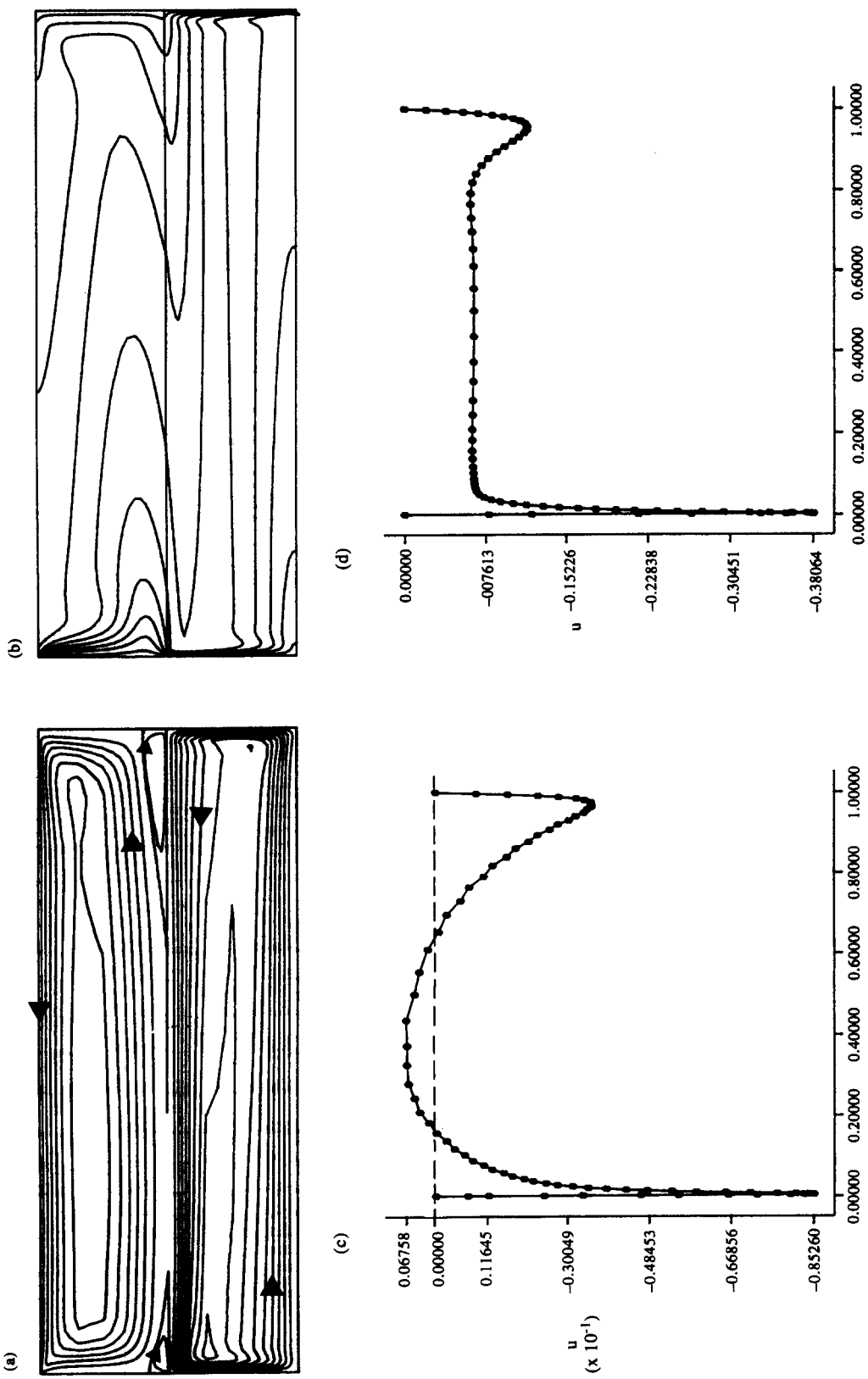

Fig. 4. Fluorinert FC75–ethylene glycol system for $\Delta T = 10$ K at 1 g: $Gr_1 = 2.8 \times 10^7$, $Ma_1 = 3.5 \times 10^5$, $Pr_1 = 23.38$, $Ca_{01} = 2.34 \times 10^{-2}$, $Gr_2 = 2.3 \times 10^4$, $Ma_2 = 2.3 \times 10^4$, $Pr_2 = 200.9$, $Ca_{02} = 2.39 \times 10^{-1}$ and $Fr = 1.81 \times 10^{-4}$. Streamlines (a), isotherms (b), and horizontal velocity profiles along the liquid–liquid interface (c) and the free surface (d). $\Psi_{Max} = 3.34 \times 10^{-3}$; $\Psi_{min} = -2.34 \times 10^{-4}$.

The surface velocity profile [Fig. 3(d)] reflects these effects: only one peak located near the cold wall occurs. An almost linear temperature gradient exists in the central part of the free surface; the latter produces primarily two regions of nearly constant acceleration. The magnitude of the velocity peak is 2.5 times larger than at the centre: $u_{fs,max} \approx 2.5u_{fs}(L/2)$ (this ratio is over 5 with water, but about 2.5 with respect to the peak that appears near the hot wall). The most notable change in the vicinity of the liquid–liquid interface is that the separation zone, i.e. the shear layer between the two co-rotating cells, generated in the upper layer in the case of the fluorinert–water system is extremely thin compared to the fluorinert–ethylene glycol system. Moreover, the sign of the horizontal velocity profile along the liquid–liquid interface shows that the shear is generated mostly in the lower layer [Fig. 3(c)]: this velocity profile indicates that the motion is directed from the cold wall, toward the hot one over a length of $2L/3$ in the central region which is in opposition to the thermocapillary forces generated along this interface. Thus, interfacial tension driven motion occurs only close to both active walls [see also Fig. 3(c)]. The sharpness of the maximum velocity peak near the cold wall is more pronounced in the fluorinert–water system at the liquid–liquid interface. A similar temperature gradient occurs near the cold wall in both systems, but less pronounced with ethylene glycol than with water. At this intermediate interface one can again notice a much stronger effect of the thermocapillary forces near the hot wall in the fluorinert–water system since the ratio between the two horizontal velocity peaks is over two with ethylene glycol ($u_{fs\text{-}cold,max} > 2u_{fs\text{-}hot,max}$) and less than 1.4 with water ($u_{fs\text{-}cold,max} < 1.4u_{fs\text{-}hot,max}$). The magnitude of deformation of both interfaces is insignificant as it is less than 1/4000, even less than with water.

As described in Part I (Section 5.1) in the fluorinert–water system the buoyancy term is 22 times larger in the lower layer which is a slightly more viscous fluid ($\mu_{FC75} \approx 1.4\mu_{water}$); this is one of the primary reasons for the occurrence of the shear layer zone in the upper layer. In the fluorinert–ethylene glycol system the buoyancy term is only 5.5 times larger in the lower layer, which is a much less viscous fluid ($\mu_{ethylene\ glycol} \approx 15\mu_{FC75}$). The highly viscous nature of the upper layer leads to the occurrence of the shear layer underneath the liquid–liquid interface.

Table 1 contains a comparison of characteristic velocities between the single layer configuration filled with fluorinert FC75, the various fluorinert FC75–water system results (with or without heat loss at the free surface) and the fluorinert FC75–ethylene glycol system. If one rates the encapsulant quality of the upper layer by the amount it minimizes the flow in the lower layer, ethylene glycol is a better encapsulant at 1 g: at $\Delta T = 1.1$ K, the maximum velocity in the lower layer is reduced by 31%. It is reduced by a ratio of 6 when the gas above the fluorinert is replaced by a layer of water. A secondary result is the reduction by 4 of the maximum velocity in the encapsulant layer when replacing water by ethylene glycol. Moreover a strong effect of the thermal boundary condition applied at the free surface is seen: convective heat loss ($Nu_2 = 5$) reduces the maximum velocity by 22% in the upper layer and by 14% in the lower layer.

When the differential temperature between the walls is increased to $\Delta T = 10$ K (viz. $Gr_1 = 2.8 \times 10^7$, $Ma_1 = 3.5 \times 10^5$, $Gr_2 = 2.3 \times 10^4$, $Ma_2 = 2.3 \times 10^4$), a strong convective type solution results in the upper layer [Fig. 4(a–d)]. (However, one must be cautioned that this steady solution may be unstable and a transient solution evolve.) At temperature gradients larger than $\Delta T = 3$ K we observe a more vigorous motion in the upper layer, but still weaker than in the lower one. In the lower layer the thermal boundary layers at the lateral boundaries are more pronounced. Despite 35% of the overall horizontal temperature gradient occurring in the vicinity of the cold wall, the maximum velocity in the lower layer is still located inside the descending flow along the cold wall, showing a weaker influence of the thermocapillary forces than in the fluorinert–water system where this maximum occurs on the liquid–liquid interface for $\Delta T > 0.36$ K. Figure 4(a, c) shows that the shear layer between the motion of the two layers is generated underneath the liquid–liquid interface only along half of the length (where extremely slow velocities appear on the velocity profile), and above near the active walls. At the free surface, some thermocapillary effects encountered with the fluorinert–water system are a sharp velocity peak located close to the cold wall where the velocities are the largest in the cavity, and a fluid acceleration near the hot wall that bends the streamlines upward [Fig. 4(a, d). Concomitant with these two effects, 65% of the global temperature gradient ΔT occurs close to the cold wall, and 20% of it occurs near the hot wall. In between a linear temperature profile and a uniform velocity profile develop. The magnitude of deformation of both moving interfaces amounts to 1/250 of the fluid depth of each layer.

CONCLUSION

This numerical study investigated the flow and concomitant thermal transport in an open cavity containing two immiscible, shallow layers of high Prandtl number liquids: mainly a fluorinert FC75–water system. A large influence of the thermal boundary condition imposed at the free surface is shown: taking into account heat loss at the top surface can change the nature of the flow in the upper layer and reduce the motion in the lower layer. Ethylene glycol appears to be a better encapsulant liquid than water if the comparison criterion is the minimization of fluid motion in the lower layer.

Acknowledgements—We wish to acknowledge Professor J. Koster and A. Prakash for collaboration during the course of this work, and P. Bontoux and E. Crespo del Arco for interesting discussion. We wish to thank also the support of the European Space Agency (through a Fellowship to J.-P.F.), of the Centre National d'Etudes Spatial (through a Fellowship to J.-P.F.), of the Center for Low-Gravity Fluid Mechanics and Transport Phenomena, of the National Science Foundation (grant CTS-91-20673 to R.L.S.), and of the GDR-MFN (Groupement de Recherche de Mécanique des Fluides Numérique G0138-CNRS).

REFERENCES

1. J. N. Koster, A. Prakash, D. Fujita and T. Doi, Bénard and Marangoni convection in immiscible liquid layers, *ASME 28th National Heat Transfer Conf.*, 9–12 August, San Diego, CA (1992).
2. J. N. Koster, A. Prakash, T. A. Campbell and A. Pline, Analysis of convection in immiscible liquid layers with novel particle tracking velocimetry, *ASME* 1992 *WAM*, 13 November, Anaheim, CA (1992).
3. M. Engelman, *FIDAP Users Manual*. Fluid Dynamics International, Evanston, IL, (1990).
4. A. Chait, Private communication, NASA Lewis, Cleveland, OH (1992).